applied sciences

MDPI

Article

Functionally Graded AISI 316L and AISI H13 Manufactured by L-DED for Die and Mould Applications

Marta Ostolaza *, Jon Iñaki Arrizubieta, Aitzol Lamikiz and Magdalena Cortina

Department of Mechanical Engineering, University of the Basque Country, Plaza Torres Quevedo 1, 48013 Bilbao, Spain; joninaki.arrizubieta@ehu.eus (J.I.A.); aitzol.lamikiz@ehu.eus (A.L.); magdalena.cortina@ehu.eus (M.C.)

* Correspondence: marta.ostolaza@ehu.eus; Tel.: +34-946-017-347

Featured Application: In this work, AISI 316L stainless steel and AISI H13 tool steel Functionally Graded Material is manufactured by L-DED for repair and coating applications in the die and mould industry. Resulting quality is evaluated and discussed.

Abstract: Tooling in the die and mould industry is subjected to high-wear and high-temperature environments, which often leads to the premature failure of this high-added-value tooling. When severe damage occurs, an alternative to replacing the whole component consists of the repair by laser-directed energy deposition (L-DED). For that end, intermediate layers are commonly employed as buffer material, where introducing a functionally graded material (FGM) might be beneficial to avoid material incompatibilities and improve the overall performance of the tooling. In the present work, an FGM composed of gradient AISI 316L to AISI H13 has been manufactured, and its microstructure and hardness analysed. Firstly, cracking owing to the formation of brittle intermediate phases has been detected. Secondly, an increase of the hardness and a decrease of the corrosion resistance has been observed when transitioning from AISI 316L to AISI H13. Thirdly, despite the FGM composition evolving linearly, nonlinear material properties such as hardness and corrosion have been observed, which are conditioned by the microstructure formed during the L-DED process and the nonlinear influence of the composition of steel on such properties. Consequently, nonlinear compositional gradients are recommended if linear mechanical properties are to be obtained in the case of steel FGMs.

Keywords: functionally graded materials; stainless steel; hot-work tool steel; Laser DED; repair; coatings; die and mould industry; tooling

Citation: Ostolaza, M.; Arrizubieta, J.I.; Lamikiz, A.; Cortina, M. Functionally Graded AISI 316L and AISI H13 Manufactured by L-DED for Die and Mould Applications. *Appl. Sci.* **2021**, *11*, 771. https://doi.org/10.3390/app11020771

Received: 22 December 2020
Accepted: 13 January 2021
Published: 15 January 2021

1. Introduction

1.1. Introduction to L-DED Processes

Additive manufacturing (AM) technologies have emerged as an alternative to traditional manufacturing processes to produce complex, fully dense, and functional parts [1]. Additive processes were originally conceived as a tool to provide a quick representation of components, that is, rapid prototyping. However, owing to the significant advances in AM and materials development, the paradigm of AM has shifted to the manufacturing of end products [2]. Moreover, AM's ability to manufacture intricate parts, unachievable through conventional manufacturing methods, has led to these technologies being adopted in aerospace, medical, energy, and automotive industries for the production of high-performance components, therefore reaching a critical acceptance level in the industry [3].

Among the many technologies developed within the metal AM envelope, directed energy deposition (DED) excels. According to the International Standard ISO/ASTM 52900:2015, DED processes are those "additive manufacturing processes in which focused thermal energy is used to fuse materials by melting as they are being deposited" [4]. Among

DED technologies, powder-based laser-DED (L-DED) is commonly used in the industry [5]. In powder-based L-DED, a laser beam is focused onto the substrate surface, where a melt pool is created. Feedstock in the powder form is simultaneously injected under a protective atmosphere, which avoids the oxidation phenomenon (Figure 1). The rapid solidification of the molten metal inherent to this process allows unique microstructures and phases to be formed, unachievable by equilibrium cooling [6]. As far as the application field of L-DED is concerned, and although it is capable of manufacturing fully functional end-parts, nowadays it is mostly employed for the remanufacture, repair, and coating of high-added-value parts in the aerospace or the die and mould industry [1]. In fact, the highly localised energy input of the laser provides a strong metallurgical bond between the added material and the substrate, while the base material retains its mechanical properties unimpaired due to the reduced heat-affected zone [7].

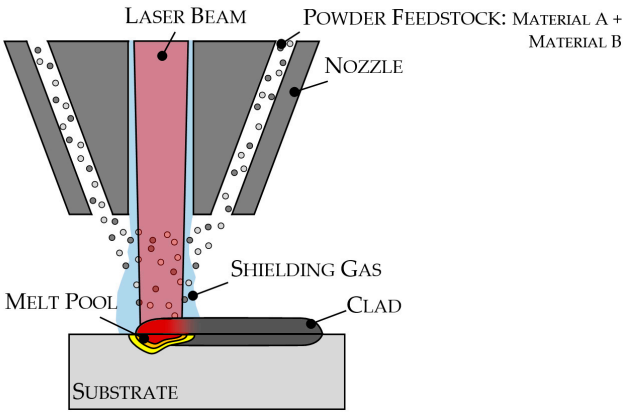

Figure 1. Working principle of laser-directed energy deposition (L-DED) for multimaterial deposition.

In the case of the die and mould industry, enhanced performance of the tooling and extended lifetime can be obtained by cladding wear and corrosion resistant coatings onto the dies/moulds [8]. On the other hand, refurbishment of the high-added-value tools to restore their functionality is also possible [9]. More specifically, L-DED enables the repair of tools for the hot-stamping process, extrusion, or casting process [10], where components are subjected to harsh corrosive, erosive, and wear conditions [11]. For this purpose, it is common practice to employ intermediate buffer layers to avoid cracking due to internal stresses and improve the weldability of materials [12], as demonstrated by Cortina et al. [13], who used AISI 316L stainless steel as an intermediate material when depositing AISI H13 hot-work tool steel over CR7V-L hot-work tool steel. In summary, repair of high-added-value components in the die and mould sector is of great interest for the industry; material compatibility issues in refurbishing need to be addressed by proposing new methodologies that incorporate advanced manufacturing techniques, such as multimaterial and functionally graded L-DED.

Once it is established that L-DED has the capability of processing different metals such as tool steels, stainless steels, titanium alloys, nickel alloys, and copper alloys [1], it is worth highlighting that it also has the capability of working with several materials simultaneously (Figure 1), allowing for multimaterial components and graded structures to be manufactured. In the literature, authors agree that one of the main advantages of this technology is its capacity for in situ mixing of different materials [2,14,15]. This feature allows for locally tailored material properties, including transition joints when joining dissimilar metals, in situ manufacturing of composites, and alloying [14]. This possibility, therefore, enables integrating different functionalities in one part and enhancing its performance as it permits proper material design in one single component [16]. In this manner, a new material-centric fabrication paradigm is made available, characterised by pointwise control of the composition and material structure [17].

1.2. Metal Functionally Graded Materials and Applications to the Die and Mould Industry

Although functionally graded materials (FGMs) were originally designed for heat-resistant applications [18,19], nowadays FGMs are also employed for the control of deformation, pressure, wear, and corrosion, as well as for replacing sharp material transitions in which high stresses are generated [20]. Traditionally, FGMs have been mostly confined to developing ceramic coatings and composite materials [21], while little attention has been given to grading metallic materials. However, with the development of AM processes, such as the aforementioned L-DED [22], FGMs of complex metallic gradients of dissimilar alloys have become available. Obtaining good metallurgical bonds between dissimilar alloys is not trivial; in fact, complete solubility over all compositions and temperatures is not common in binary alloys, and it is much more complex in ternary or multicomponent alloys [23]. This issue might be addressed by introducing compositional gradients. Still, the manufacture of FGMs using L-DED is not without its challenges, mainly, lack of solubility, atomic structure mismatch, variation in the coefficient of thermal expansion (CTE), and formation of brittle intermetallic phases leading to cracking along the graded composition [24]. Meng et al. [25] proposed laser synchronous preheating as a way of reducing residual stresses during the deposition process for avoiding the cracking phenomenon, as solidification cracking occurred when manufacturing graded Inconel 625 to AISI 316L samples. They effectively avoided cracks in the preheated samples, while cracking was found in the non-preheated samples from 90% 316L to 70% 316L. Zhang et al. [8], on the other hand, studied the microstructure, hardness, and tensile fracture of AISI 316L to Inconel 625 samples. Firstly, they observed gradient hardness along the graded region, which matched the microstructure. Also, the fracture in the tensile testing occurred in the AISI 316L section, while the interfaces survived the testing, owing to the graded transition. Su et al. [26] studied the microstructure of AISI 316L to Inconel 718 graded samples and found that austenitic formation was promoted in the graded region, leading to the loss of hardness in certain areas. Carrol et al. [24] analysed AISI 304L to Inconel 625 gradient samples, where they found cracks of several microns due to the formation of carbides in the graded section. In addition, Nam et al. [27] compared deposition of AISI 316 onto mild steel substrate with the Fe/AISI 316 gradient deposition and found that while many pores and cracks were observed in the sharp transition, no cracking was detected in the graded sample. Finally, Fessler et al. [28] fabricated an Invar to AISI 316L graded part and found that while the composition distribution was linear, the hardness along the graded sample was distinctly nonlinear and justified it with the hardness not increasing linearly with the carbon content in the stainless steels.

To sum up, although some research on FGMs of metallic alloys by L-DED has been carried out, little work on FGMs applied to the die and mould sector has been published, and no studies on FGMs with AISI H13 tool steel have been carried out. Therefore, with the aim of overcoming this gap, in the present work, an analysis of the microstructure and the mechanical properties of AISI 316L/AISI H13 FGM was performed, as this combination of materials has a potential use in the repair and coating of tooling for hot-stamping processes. For that purpose, graded samples with 20% composition intervals from 100% AISI 316L to 100% AISI H13 have been manufactured using powder-baser L-DED. Then, a metallographic analysis has been performed to assess the quality of the deposited material, the state of the interfaces, and the microstructures generated. Finally, microhardness measurements have been acquired along the coatings to evaluate the mechanical properties of the deposited material.

2. Materials and Methods

2.1. Materials

All the experiments described in this work have been carried out in a 5-axis laser processing centre, which has a Rofin FL010 Yb:YAG fibre laser source coupled to it. The maximum power of the laser source is 1 kW and the emitting wavelength is 1064 nm. Finally, the diameter of the laser spot on the surface of the workpiece is 1.8 mm. As far as

the feeding system is concerned, a Sulzer Metco Twin 10-C powder feeder was employed, whose two independent hoppers allow for multimaterial and graded deposition, and the EHU/Coax 2015 nozzle was used for the delivery of the powder into the melt pool. Finally, argon was used as both carrier and shielding gas. As far as the powder delivery is concerned, each material, that is AISI H13 and AISI 316L, was contained in one of the individual hoppers of the powder feeder and it was transported by the carrier gas to the L-DED nozzle. In an intermediate point between the powder feeder and the nozzle, both powders came together by means of a Y fitting, as shown in Figure 2. Then, both materials were further mixed in the nozzle to ensure a homogeneous material mixture.

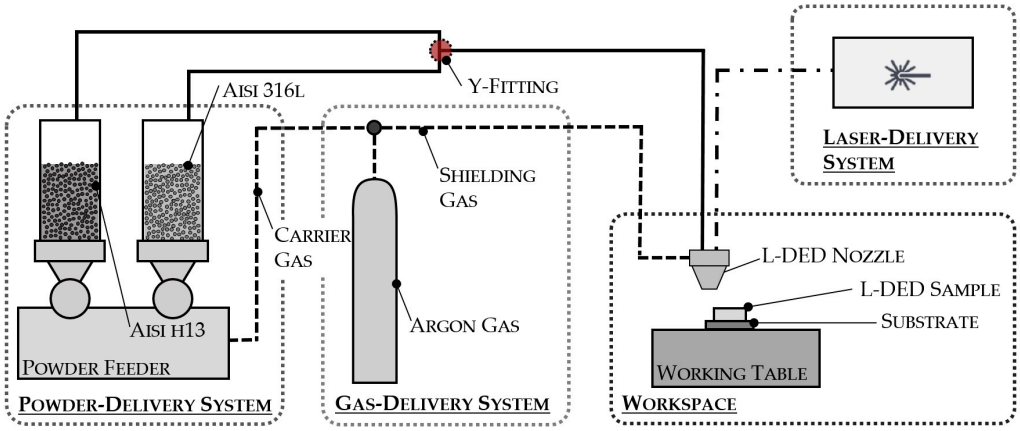

Figure 2. Setup of the L-DED process.

The composition of the materials employed in the experiments is detailed in Table 1 [29–31]. AISI H13 hot-work tool steel and AISI 316L low-carbon stainless steel powders were employed as feedstock materials to produce the FGM deposit over an AISI 1045 mild steel substrate. The powder particle size of the feedstock employed was 53–150 µm for the AISI H13 powder and 45–125 µm for the AISI 316L powder. The dimensions of the substrates were 70 × 70 × 15 mm^3 and layers of 30 × 30 mm^2 were deposited onto them. In order to ensure the consistency of the proposed methodology, two samples were manufactured, following the same deposition strategy and process parameters detailed in the hereafter section.

Table 1. Chemical composition of the employed materials (wt.%).

Material	C	Cr	Mo	Ni	V
AISI H13	0.41	5.12	1.33	-	1.13
AISI 316L	<0.03	16.50–18.50	2.00–2.50	10–13	-
AISI 1045	0.42–0.50	-	-	-	-
Material	**Si**	**Mn**	**P**	**S**	**Fe**
AISI H13	0.80	0.25	0.010	<0.010	Bal.
AISI 316L	<1.00	<2.00	<0.045	<0.015	Bal.
AISI 1045	-	0.60–0.90	<0.040	<0.050	Bal.

2.2. L-DED Process

Regarding the L-DED deposition strategy, a contour and infill strategy has been selected in order to improve the dimensional accuracy of the manufactured samples. Also, an alternating zigzag pattern has been followed for the successive layers, as shown in Figure 3. Note that the trajectory was not continuous during the zigzag path, as the laser was turned off in every change of direction (discontinuous path in Figure 3). Regarding the transition between layers, once one layer was completed, the laser was turned off and the nozzle moved up to continue with the following layer. As far as the composition of the layers deposited is concerned, 20% composition intervals have been applied, starting

with 100% AISI 316L stainless steel to 100% AISI H13 tool steel. A single layer of each intermediate composition and three layers of the unmixed materials have been deposited, as depicted in Table 2.

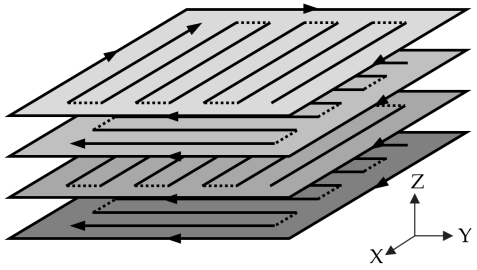

Figure 3. L-DED deposition strategy.

Table 2. Chemical composition of the deposited layers.

Layer	Composition (wt.%)
1–3	100% AISI 316L
4	80% AISI 316L + 20% AISI H13
5	60% AISI 316L + 40% AISI H13
6	40% AISI 316L + 60% AISI H13
7	20% AISI 316L + 80% AISI H13
8–10	100% AISI H13

In addition, the process parameters employed are indicated in Table 3. Taking as reference the optimised L-DED process parameters for the single materials, the parameters for the intermediate layers have been calculated by linear interpolation according to the composition of the added material in each case. Regarding layer thickness, as a result of the combination of the specific configuration of the powder injection nozzle, the laser spot, and the optimal process parameter window, a constant layer thickness of 0.38 mm has been obtained for each layer along the samples. So, for this particular case, the process parameters have been carefully chosen so that the aforementioned constant layer thickness is obtained for each individual material combination.

Table 3. L-DED parameters employed.

Layer	Power (W)	Scan Velocity (mm·min^{-1})	Powder Flow Rate (g·min^{-1})	
			AISI 316L	AISI H13
1–3	625	550	5.00	0.00
4	620	530	4.00	0.66
5	615	510	3.00	1.32
6	610	490	2.00	1.98
7	605	470	1.00	2.64
8–10	600	450	0.00	3.30

Finally, it should be noted that the substrate was simply supported onto the working table, as shown in Figure 2. In fact, as no external forces during the L-DED process nor movement in the 5-axis was expected, there was no need for additional clamping to ensure that the substrate would not move during the material deposition. As far as machine kinematics are concerned, movements in the X and Y directions were given by the working table, while the Z direction was given by the L-DED head. In Figure 4, the resulting FGM samples are shown. Additionally, a schematic illustration of the fabricated and the resulting sample with dimensions are also depicted.

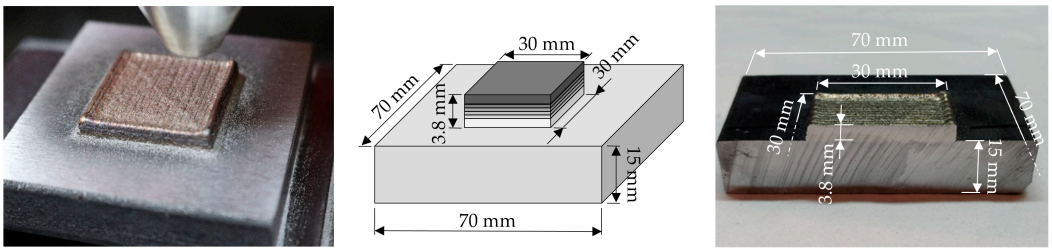

(**a**) (**b**) (**c**)

Figure 4. Dimensions of the manufactured samples: (**a**) functionally graded material (FGM) sample during the L-DED process, (**b**) schematic illustration of the fabricated FGM sample with dimensions, and (**c**) fabricated FGM sample with dimensions.

2.3. Metallographic Preparation, Microstructure Analysis, and Hardness Measurement

Once the sample was produced, the central cross-section has been selected to be analysed and, for that purpose, it has been cut, encapsulated, and ground and polished following the appropriate metallographic procedure. In addition, the sample has been etched with 10% oxalic acid solution at 20 V and Marble's reagent to reveal the microstructure.

Then, a LEICA DCM 3D confocal microscope has been used for defect inspection and microstructure analysis, which has been carried out layer by layer.

Finally, a Future Tech FM 800 microhardness tester has been employed for hardness measurements. Indentations every 0.15 mm have been done and four hardness profiles along the Z building direction of the samples have been extracted, two in each sample. For the indentations, 2.9 N applied load and 12 s dwell time have been selected.

3. Results

In this section, the results obtained in the experimental testing are presented and discussed. When analysing the central cross-section of the sample from a macroscopic perspective, severe cracking, mostly on the right side of the section, was observed (Figure 5). In addition, several lack-of-fusion defects were also identified. Apparently, this cracking phenomenon was not related to the formation of carbides, as the hardness was not found to be particularly high in the cracked areas. On the contrary, it was attributed to the formation of the brittle sigma phase, which is common in stainless steels. According to Bobbio et al., subsequent heating and cooling cycles in L-DED may promote the growth of the sigma phase, leading to cracking of the component [32]. In addition, it has been reported in the literature that FGMs which grade from metals or alloys with different crystal structures (as it is in this case) present a higher tendency for the generation of macrocracks [3].

Figure 5. Macro metallographic inspection of the deposited FGM sample.

Additionally, graded corrosion resistance was not observed when etching the sample, in contrast with previous works when functionally graded Stellite-6 and tungsten carbide metal matrix composite samples were manufactured, and some sort of linear corrosion

resistance was obtained. Lower layers were just slightly etched, whereas the intermediate layers were further etched and the upper layers were more prominently etched [33]. In the present case, the lower and intermediate layer were just slightly etched while the upper three layers, which correspond to 100% unmixed AISI H13, showed a strong reaction to the etching procedure. This is due to the fact that corrosion resistance was not linear for the chromium content range present in the sample, e.g., from 5.12% in the AISI H13 to 18.50% in the AISI 316L, as depicted in Figure 6 (note the logarithmic scale).

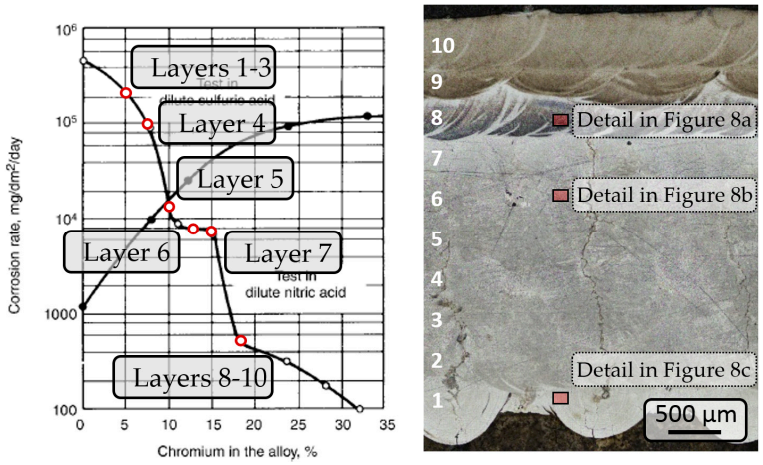

Figure 6. Corrosion resistance of each layer as a function of chromium content of the alloy.

On the other hand, the microstructure of the sample also evolved along the FGM. Initially, three layers of AISI 316L were deposited, which are constituted by 90% austenite and 10% ferrite. Then, the ferrite content decreased gradually until the sixth layer, which should be constituted by austenite. Finally, the last three layers were composed of AISI H13, which corresponded to martensite and austenite. These theoretical microstructural constituents were estimated based on the Schaeffler diagram, shown in Figure 7 [34], and validated with the microscope images shown in Figure 8. For that purpose, nickel and chromium equivalents were calculated, according to the following formulae [35]:

$$C_{eq} = Cr + 2{\cdot}Si + 1.5{\cdot}Mo + 5{\cdot}V, \quad (1)$$

$$Ni_{ea} = Ni + 0.5{\cdot}Mn + 30{\cdot}C. \quad (2)$$

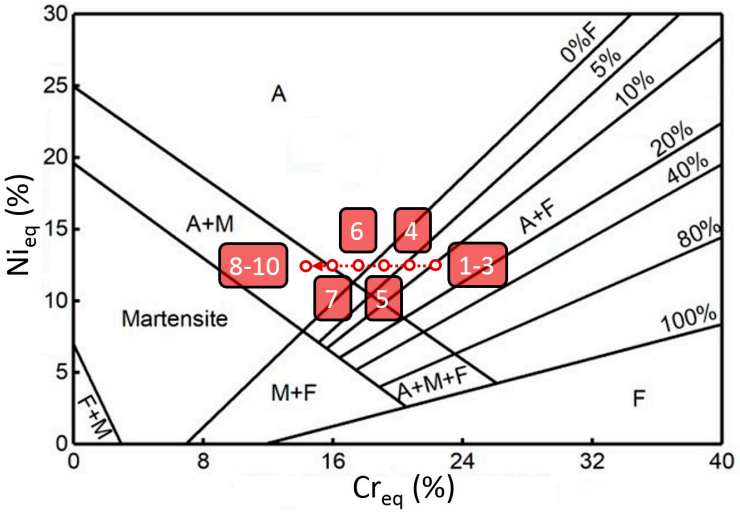

Figure 7. Schaeffler diagram for microstructural constituent estimation [36].

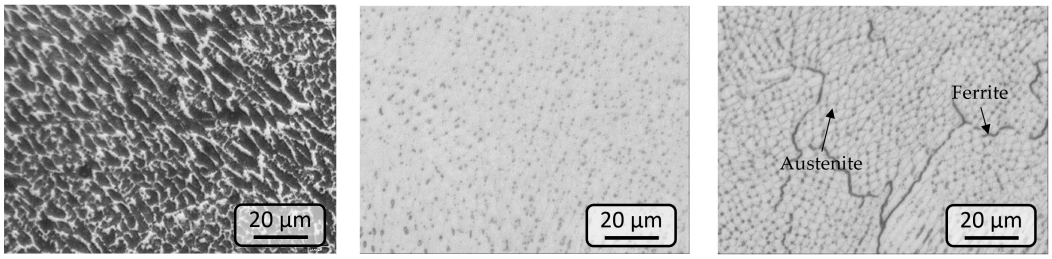

Figure 8. Microstructure details of the FGM sample along the gradient (specific location shown in Figure 6): (**a**) eighth layer, 100% AISI H13 with its microstructure constituted by martensite and austenite, (**b**) sixth layer, 40% AISI 316L and 60% AISI H13 with mostly austenitic microstructure, (**c**) first layer, 100% AISI 316L with austenite and ferrite constituted microstructure.

Finally, as far as the hardness of the sample is concerned, a nonlinear hardness increase has been observed from the first layers and up to the last three layers, showing typical cladded AISI H13 hardness values. In Figure 9, the hardness values measured along the building direction of the FGM are shown, and at the same time compared with the maximum attainable hardness of the steels calculated from the carbon content according to [37,38]. It can be observed that the upper layers, corresponding to the unmixed tool steel, reached the maximum attainable hardness values owing to the formation of martensite and the characteristic precipitation of the carbides that constitute AISI H13. However, in the graded intermediate layers, the hardness decreased abruptly rather than in a gradual manner, as could be expected based on carbon content of the added material. This occurred because the resulting microstructure was also conditioned by nickel and chromium equivalents, as it is detailed in the Schaeffler diagram shown in Figure 6. Intermediate graded compositions promoted austenite formation and, therefore, the resulting hardness was significantly reduced. Also, due to the reduced carbon content, carbide formation may be impeded and, consequently, the hardness reduced.

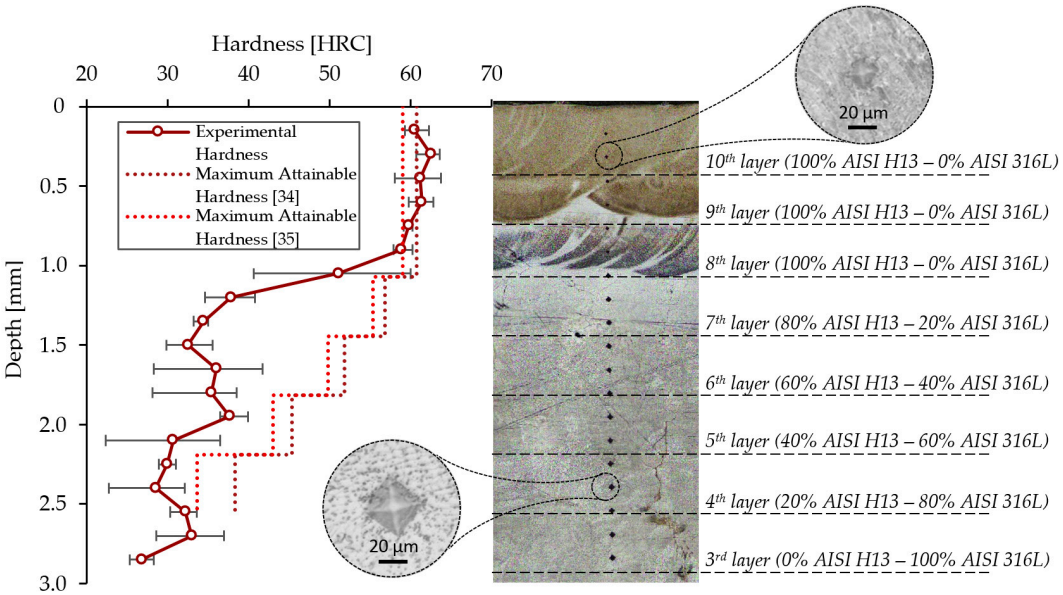

Figure 9. Hardness of the AISI 316L to AISI H13 FGM sample, with respect to the maximum attainable hardness achieved by steels based on the carbon content.

These results go in line with the conclusions reached by DebRoy et al. [3], which stated that hardness in FGMs does not necessarily increase linearly in graded materials with different crystal structures. A similar phenomenon occurred in the Invar-Stainless

Steel graded part fabricated by Fessler et al. [28], where the hardness did not follow a linear behaviour and increased abruptly when reaching the tool steel area, although they attributed this phenomenon to the low carbon content of the added material.

4. Discussion

In the present work, FGM samples constituted by AISI H13 hot-work tool steel and AISI 316L low carbon stainless steel have been produced by means of L-DED. Starting from 100% AISI 316L, a graded structure has been built until 100% AISI H13 composition has been reached, with 20% composition intervals. The objective of the study was to perform a microstructural analysis and to understand how the mechanical properties of the FGM evolved along the gradient. For that aim, a metallographic analysis and microhardness measurements in different areas of the FGM have been carried out. The following conclusions can be drawn from the obtained results:

- Regarding metallurgical integrity of the added material, severe cracking and several lack-of-fusion defects have been observed. The first was concluded to be due to the brittle sigma phase formation. This issue has been also reported in the literature and it is associated with the successive heating and cooling cycles inherent to the L-DED process, which tend to promote sigma phase growth.
- The corrosion resistance of the graded structure did not follow a linear behaviour. The initial 100% AISI 316L and the intermediate layers with mixed composition showed similar corrosion resistance, while the upper layers composed of AISI H13 were strongly affected by the etching process. This was due to the nonlinearity of corrosion resistance according to chromium content range present in this work.
- As far as the microstructure of the FGM is concerned, it depended on the composition of the deposited materials and, consequently, a variation along the sample has been observed. Lower layers composed of AISI 316L and low AISI H13 contents, showed an austenite + ferrite microstructure; while intermediate layers with higher AISI H13 contents had an austenitic microstructure; and, finally, AISI H13 layers presented a martensite + austenite microstructure.
- The aforementioned microstructure variation strongly conditioned the hardness of the graded sample, and consequently, a nonlinear hardness profile has been measured. In fact, the hardness abruptly increased when reaching the upper three layers composed of AISI H13, while lower values of hardness were present in the rest of the FGM.

5. Conclusions

After analysing the obtained results, it was concluded that a linear variation of the constituents does not always result in linear variation of the properties. Therefore, if properties varying in a linear manner are to be obtained, nonlinear compositional gradients should be considered in the case of working with steel FGMs. In addition, nonlinear and precisely selected compositions might help avoid the formation of sigma phase, which promotes cracking, by staying away from conflicting compositions.

To end, although it is beyond dispute that hot-work tool steels in combination with stainless steels have a direct application in the die and mould industry, where they can serve as an innovative repair and coating methodology for high-added-value tools, it is suggested that further research needs to be conducted on this type of FGM as future work.

Author Contributions: Conceptualization, M.C., J.I.A. and A.L.; methodology, M.C., M.O., J.I.A. and A.L.; investigation, M.O.; data curation, M.O.; writing—original draft preparation, M.O.; writing—review and editing, J.I.A. and A.L.; supervision, J.I.A. and A.L.; project administration, A.L.; funding acquisition, A.L. All authors have read and agreed to the published version of the manuscript.

Funding: This research was funded by the Basque Government (Eusko Jaurlaritza) under the ELKARTEK Program, QUALYFAM project, grant number KK-2020/00042 and Spanish Ministry of Industry and Competitiveness under the PID2019-109220RB-I00 ALASURF project.

Institutional Review Board Statement: Not applicable.

Informed Consent Statement: Not applicable.

Data Availability Statement: The data presented in this study are available on request from the corresponding author.

Acknowledgments: The authors would like to thank Xabier Martínez for his technical support during the experimental testing.

Conflicts of Interest: The authors declare no conflict of interests.

References

1. Arrizubieta, J.I.; Ukar, O.; Ostolaza, M.; Mugica, A. Study of the Environmental Implications of Using Metal Powder in Additive Manufacturing and Its Handling. *Metals* **2020**, *10*, 261. [CrossRef]
2. Han, D.; Lee, H. Recent advances in multi-material additive manufacturing: Methods and applications. *Curr. Opin. Chem. Eng.* **2020**, *28*, 158–166. [CrossRef]
3. DebRoy, T.; Wei, H.L.; Zuback, J.S.; Mukherjee, T.; Elmer, J.W.; Milewski, J.O.; Beese, A.M.; Wilson-Heid, A.; De, A.; Zhang, W. Additive manufacturing of metallic components—Process, structure and properties. *Prog. Mater. Sci.* **2018**, *92*, 12–224. [CrossRef]
4. ISO/ASTM. 52900: 2015 Additive Manufacturing—General Principles—Terminology. Available online: https://www.iso.org/obp/ui/#iso:std:iso-astm:52900:ed-1:v1:en (accessed on 14 December 2020).
5. Loh, G.H.; Pei, E.; Harrison, D.; Monzón, M.D. An overview of functionally graded additive manufacturing. *Addit. Manuf.* **2018**, *23*, 34–44. [CrossRef]
6. Bandyopdhyay, A.; Heer, B. Additive manufacturing of multi-material structures. *Mater. Sci. Eng. R Rep.* **2018**, *129*, 1–16. [CrossRef]
7. Siddiqui, A.A.; Dubey, A.K. Recent trends in laser cladding and surface alloying. *Opt. Laser Technol.* **2021**, *134*, 106619. [CrossRef]
8. Zhang, X.; Chen, Y.; Liou, F. Fabrication of SS316L-IN625 functionally graded materials by powder-fed directed energy deposition. *Sci. Technol. Weld. Join.* **2019**, *24*, 504–516. [CrossRef]
9. Dass, A.; Moridi, A. State of the Art in Directed Energy Deposition: From Additive Manufacturing to Materials desing. *Coatings* **2019**, *9*, 418. [CrossRef]
10. Klocke, F.; Arntz, K.; Teli, M.; Winands, K.; Wegener, M.; Oliari, S. State-of-the-art Laser Additive Manufacturing for Hot-work Tool Steels. *Procedia CIRP* **2017**, *63*, 58–63. [CrossRef]
11. Saboori, A.; Psicopo, G.; Lai, M.; Salmi, A.; Biamino, S. An investigation on the effect of deposition pattern on the microstructure, mechanical properties and residual stress of 316L produced by Directed Energy Deposition. *Mater. Sci. Eng. A* **2020**, *780*, 139179. [CrossRef]
12. Yan, L.; Chen, Y.; Liou, F. Additive manufacturing of functionally graded metallic materials using laser metal deposition. *Addit. Manuf.* **2020**, *31*, 100901. [CrossRef]
13. Cortina, M.; Arrizubieta, J.I.; Calleja, A.; Ukar, E.; Alberdi, A. Case Study to Illustrate the Potential of Conformal Cooling Channels for Hot Stamping Dies Manufactured Using Hybrid Process of Laser Metal Deposition (LMD) and Milling. *Metals* **2018**, *8*, 102. [CrossRef]
14. Brueckner, F.; Riede, M.; Müller, M.; Marquardt, F.; Willner, R.; Seidel, A.; Lopéz, E.; Leyens, C.; Beyer, E. Enhanced manufacturing possibilities using multi-materials in laser metal deposition. *J. Laser Appl.* **2018**, *30*, 032308. [CrossRef]
15. Ituarte, I.F.; Boddeti, N.; Hassani, V.; Dunn, M.L.; Rosen, D.W. Design and additive manufacture of functionally graded structures based on digital materials. *Addit. Manuf.* **2019**, *30*, 100839. [CrossRef]
16. Yao, X.; Moon, S.K.; Bi, G.; Wei, J. A multi-material part design framework in additive manufacturing. *Int. J. Adv. Manuf. Tech.* **2018**, *99*, 2111–2119. [CrossRef]
17. Yu, H.Z.; Cross, S.R.; Schuh, C.A. Mesostrucure optimization in multi-material additive manufacturing: A theoretical perspective. *J. Mater. Sci* **2017**, *52*, 4288–4298. [CrossRef]
18. Zhou, W.; Zhang, R.; Ai, S.; He, R.; Pei, Y.; Fang, D. Load distribution in threads of porous metal-ceramic functionally graded composite joints subjected to thermomechanical loading. *Compos. Struct.* **2015**, *134*, 680–688. [CrossRef]
19. Zhou, W.; Ai, S.; Chen, M.; Zhang, R.; He, R.; Pei, Y.; Fang, D. Preparation and thermodynamic analysis of the porous ZrO_2/(ZrO_2 + Ni) functionally graded bolted joint. *Compos. Part B-Eng.* **2015**, *82*, 13–22. [CrossRef]
20. Saleh, B.; Jiang, J.; Fathi, R.; Tareq, A.; Xu, Q.; Wang, L.; Song, D.; Ma, A. 30 Years of functionally graded materials: An overview of manufacturing methods, Applications and Future Challenges. *Compos. Part B-Eng.* **2020**, *201*, 108376. [CrossRef]
21. Zhou, W.; Zhang, R.; Fang, D. Design and analysis of the porous ZrO_2/(ZrO_2 + Ni) ceramic joint with load bearing-heat insulation integration. *Ceram. Int.* **2016**, *42*, 1416–1424. [CrossRef]
22. Kim, D.K.; Woo, W.; Kim, E.Y.; Choi, S.H. Microstrucutre and mechanical characteristics of multi-layered materials composed of 316L stainless steel and ferritic steel produced by direct energy deposition. *J. Alloys Compd.* **2019**, *774*, 896–907. [CrossRef]
23. Reichardt, A.; Shapiro, A.A.; Otis, R.; Dillon, R.P.; Borgonia, J.P.; McEnerney, B.W.; Hosemann, P.; Beese, A.M. Advance in additive manufacturing of metal-based functionally graded materials. *Int. Mater. Rev.* **2020**. [CrossRef]

24. Carroll, B.E.; Otis, R.A.; Borgonia, J.P.; Suh, J.; Dillon, R.P.; Shapiro, A.A.; Hofmann, D.C.; Liu, Z.K.; Beese, A.M. Functionally graded material of 304L stainless steel and Inconel 625 fabricated by directed energy deposition: Characterization and thermodynamic modeling. *Acta Mater.* **2016**, *108*, 46–54. [CrossRef]
25. Meng, W.; Zhang, W.; Zhang, W.; Yin, X.; Cui, B. Fabrication of steel-Inconel functionally graded materials by laser melting deposition integrating with laser synchronous preheating. *Opt. Laser Technol.* **2020**, *131*, 106451. [CrossRef]
26. Su, Y.; Chen, B.; Tan, C.; Song, X.; Feng, J. Influence of composition gradient variation on the microstructure and mechanical properties of 316 L/Inconel718 functionally graded material fabricated by additive manufacturing. *J. Mater. Process. Technol.* **2020**, *283*, 116702. [CrossRef]
27. Nam, S.; Cho, H.; Kim, C.; Kim, Y.M. Effect of Process Parameters on Deposition Properties of Functionally Graded STS 316/Fe Manufactured by Laser Direct Metal Deposition. *Metals* **2018**, *8*, 607. [CrossRef]
28. Fessler, J.; Nickel, A.; Link, G.; Priz, F. Functional Gradient Metallic Prototypes through Shape Deposition Manufacturing. In Proceedings of the International Solid Freeform Fabrication Symposium, Austin, TX, USA, 11–13 August 1997.
29. FST Flame Spray Technologies. ST H13 (DIN 1.2344) Powder Datasheet.
30. Metallied Powder Solutions SA Erasteel. Pearl® Micro 316L Datasheet.
31. MatWeb Material Property Data. Available online: http://www.matweb.com/search/datasheet.aspx?matguid=193434cf42e343fab880e1dabdb143ba&ckck=1 (accessed on 16 December 2020).
32. Boobio, L.D.; Bocklund, B.; Reichardt, A.; Otis, R.; Borgonia, J.P.; Dillon, R.P.; Shapiro, A.A.; McEnerney, B.W.; Hosemann, P.H.; Liu, Z.K.; et al. Analysis of formation and growth of the σ phase in additively manufactured functionally graded materials. *J. Alloys Compd.* **2020**, *814*, 151729. [CrossRef]
33. Ostolaza, M.; Arrizubieta, J.I.; Cortina, M.; Lamikiz, A. Study of the reinforcement phase dilution into the metal matrix in functionally graded Stellite 6 and WC metal matrix composite by Laser Metal Deposition. *Procedia CIRP* **2020**, *94*, 330–335. [CrossRef]
34. Verhoeven, J.D. *Steel Metallurgy for the Non-Metallurgist*; ASM International, Ohio: Materials Park, OH, USA, 2007; pp. 133–155. [CrossRef]
35. Sourmail, T. Stainless Steels. Available online: http://thomas-sourmail.net/stainless/ (accessed on 16 December 2020).
36. Zhou, L.; Liu, Y.; Li, Z.; Zhu, L.; Li, Y.; Xiong, A. Microstructure and properties of Fe-Cr-Ni alloy coatings on T10 steel by laser cladding. *Mater. Res. Express* **2019**, *7*, 016513. [CrossRef]
37. Payson, P. *The Metallurgy of Tool Steels*; John Wiley & Sons, Inc.: London, UK, 1962.
38. Dossett, J.; Totten, G.E. *ASM Handbook, Volume 4A, Steel Heat Treating Fundamentals and Processes*; ASM International: Materials Park, OH, USA, 2013.